CHEMMEDCHEM

CHEMISTRY ENABLING DRUG DISCOVERY

Accepted Article

Title: Discovery and pharmacophore mapping of a new low nanomolar inhibitor of P. falciparum growth

Authors: Ivan Bassanini, silvia parapini, Corinna Galli, Nadia Vaiana, Andrea Pancotti, nicoletta Basilico, Donatella Taramelli, and Sergio Romeo

To be cited as: *ChemMedChem* 10.1002/cmdc.201900526

Link to VoR: http://dx.doi.org/10.1002/cmdc.201900526

A Journal of

ChemPubSoc Europe

WILEY-VCH

www.chemmedchem.org

FULL PAPER WILEY-VCH

Discovery and pharmacophore mapping of a new low nanomolar inhibitor of *P. falciparum* growth

Ivan Bassanini,[a] Silvia Parapini,[b] Corinna Galli,[a] Nadia Vaiana,[a] Andrea Pancotti,[a] Nicoletta Basilico,[b] Donatella Taramelli,[c] and Sergio Romeo*[a]

[a] Dr. I. Bassanini 0000-0001-9589-3689; Dr. C. Galli, Dr. N. Vaiana, dr. A. Pancotti, Prof. S. Romeo 0000-0003-4692-7314
Dipartimento di Scienze Farmaceutiche
Università degli Studi di Milano
Via Mangiagalli 25, 20133, Milan, Italy
E-mail: sergio.romeo@unimi.it
[b] Dr. S. Parapini, Prof. N. Basilico
Dipartimento di Scienze Biomediche, Chirurgiche e Odontoiatriche
Università degli Studi di Milano
Via Pascal, 36, 20133 Milan, Italy
[c] Prof. D. Taramelli 0000-0001-5108-4492
Dipartimento di Scienze Farmacologiche e Biomolecolari
Università degli Studi di Milano
Via Pascal 36, 20133 Milan, Italy

Supporting information for this article is given via a link at the end of the document.

Abstract: The treatment of malaria, the most common parasitic disease worldwide and the third deadliest infection after HIV and tuberculosis, is nowadays harmed by the dramatic increase and diffusion of drug-resistance among the different species of *Plasmodium*, especially *P. falciparum* (*Pf*). In this view, the development of new antiplasmodial agents, able to act via innovative mechanisms of action, is crucial to ensure efficacious antimalarial treatments. In one of our previous communications, we described a novel class of compounds endowed with high antiplasmodial activity, characterized by a pharmacophore never described before as antiplasmodial and identified in their 4,4'-oxybisbenzoyl amide cores. Here, through a detailed structure-activity relationship (SAR) study, we deeply investigated the chemical features of the reported scaffolds and successfully built a novel antiplasmodial agent active on both chloroquine (CQ) sensitive and CQ-resistant *Pf* strains in the low nanomolar range, without displaying cross resistance. Moreover, we conducted an *in silico* pharmacophore mapping.

Introduction

Protozoan infections are parasitic diseases caused by diverse group of unicellular eukaryotes. As a noteworthy example, malaria, a mosquito borne infectious disease affecting humans and other animals, is caused by parasitic protozoa belonging to the *Plasmodium* genus, the deadliest and more common among them being *Plasmodium falciparum* (*Pf*).[1] It has been reported that the spread of malarial infections produces a massive impact on human health, causing, in 2017, 219 million clinical cases and *ca* 435000 deaths worldwide.[2] Presently, the best performing strategies of intervention against malaria are the artemisinin-based combination therapies (ACTs), in which the natural occurring sesquiterpene lactone, artemisinin, plays a key role. Unfortunately, the spread of drug resistance has been recently reported as a critical issue affecting ACTs and first line drugs in general, enhancing the need of constant monitoring the efficacy of ACTs to revise and update national malaria treatment policies.[3,4] This scenario, combined with few commercially available drugs, could eventually become a dramatic public health problem, hindering malaria treatment and highlighting the need of new antimalarials with innovative mechanism of action. In the quest for a novel approach to treat malaria, the targeting of plasmepsins (PLMs, aspartic proteases involved, among others, in the digestion of haemoglobin in the parasitic food vacuole) was at first considered by our group as a promising strategy to develop new drug candidates. To this purpose, a family of synthetic peptides characterized by the presence of a statine, a β-hydroxyl amino acid able to block the actions of PLMs, and the typical 4-aminoquinolinic ring system of the antimalarial drug chloroquine (CQ), was synthetized and its antiplasmodial activity investigated.[5–7] Recently, the finding of discrepancies in the relationship between the inhibition of PLMs and the actual inhibition of parasite growth promoted by these compounds, led us to further investigate the nature of their real pharmacophore. We substituted the statine, responsible for PLM2 inhibition, with leucine and the 4-aminoquinolinic ring system with a basic tertiary amine.[8] Among these novel drug candidates, compound 1 (Figure 1), which doesn't present any known antimalarial pharmacophoric group, showed a remarkable antiplasmodial activity both on CQ-sensitive (CQ-S) and CQ-resistant (CQ-R) *Pf* strains. Based on these results, we concluded that compound **1** must owe its activity to a new antimalarial pharmacophore, recognized as the oxybisbenzoylamide core, acting through a (new) unidentified mechanism of action.

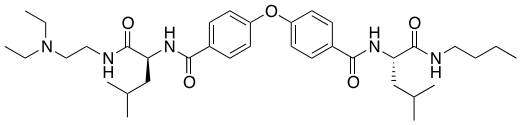

Figure 1. Compound **1** (IC_{50}: D10 350 nM, W2 314 nM; LLE: 3.01, LLE_{AT}: 0.2)

In this work, we further pursue our investigation on compound **1** by synthesizing a panel of novel, structurally-simplified analogues and conducting a detailed structure-activity relationship (SAR) study aimed at understanding the structural and chemical features promoting the nanomolar *in vitro* activity of compound **1.** Moreover, the design of the structurally-simplified analogues of **1** has been also focused on the

optimization its "*druggability*". This because the calculated ligand lipophilicity efficiency (LLE), a parameter describing the "*druglikeness"* of a compound directly correlating to its pIC_{50} and inversely to its lipophilicity[9–11], and the corresponding LLE_{AT}, the same parameter corrected for the number of heavy atoms, of compound **1** (**Figure 1**) reveled some potential drawbacks for its therapeutic application in terms of pharmacokinetics and bioavailability

Results and Discussion

Chemistry

Since a large number of compounds was needed to perform our investigation, a simple and straightforward synthetic pathway avoiding the use of protective group chemistry and intermediate purification, was designed to prepare compounds **3**-**19** and **21-31** (**Tables 1-4**).

Relying on a previously described TBTU-based coupling chemistry,[8] the central 4-4'-bisbenzoic acid core was directly coupled with a selected primary amine and, after simple work-up procedures, coupled again with another amine (**scheme 1**). The desired products were finally purified by means of reverse-phase preparative HPLC and isolated as HCl salts using a 1M HCl solution.

Compounds **25** and **26** were prepared following the synthetic strategy proposed in **scheme 2** starting from commercially available 4,4'-methylenedibenzoic and 4,4'-sulfonyldibenzoic acid, respectively, while **27** was obtained from 4,4'-(furan-2,5-diyl)bisbenzoic acid, prepared as described by Boykin *et al.* (**Table 4**).[12]

The "truncated" compound **2** (**Table 1**) was prepared from 4-phenoxybenzoic acid.

Compound **20** (**Table 3**) was obtained from **3** by alkaline hydrolysis.

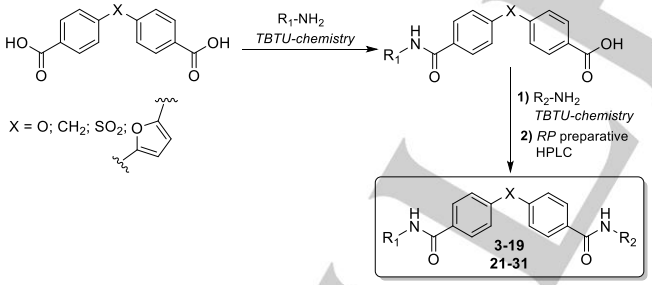

Scheme 1. Synthetic pathway towards compounds **3-19** and **21-31**.

Amines **a-m** were prepared by coupling N^{ω},N^{ω}-dialkyl-alkylen-α,ω-diamines or a primary aliphatic amine with *N*-protected α-amino acids.

Antiplasmodial activity

Compounds **2-31** were tested *in vitro* against W2, CQ-R and D10 CQ-S *Pf* strains, using CQ as reference drugs. Antiplasmodial activity was expressed as inhibition of parasite growth measuring the activity of parasite lactate dehydrogenase (pLDH).[13]

The results, expressed as IC_{50} (nM), are reported in **Tables 1-4** in which are also indicated the corresponding resistance indexes (R.I.), *i.e*. the ratios between the IC_{50} of each compound against the CQ-R and CQ-S *Pf* strains, a value suggestive of cross resistance between a compound and CQ.

In general, all the tested compounds did not show a relevant cross resistance with CQ (0.40 < calculated R.I.s < 2) confirming the similar inhibitory activity of these 4,4'-oxybisnebezoyl amides on both D10 and W2 strains describes before.[8]

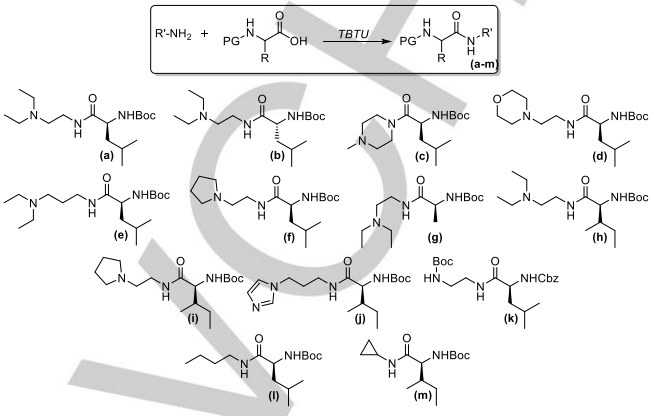

Scheme 2. Synthetic entry to amines **a**-**m**.

As a direct consequence of the chemical and conformational space covered by the highly-divergent analogues of compound **1**, the resulting *in vitro* antiplasmodial activities (IC_{50}) of **2-31** were spread between more than 10 μM and less than 1 nM.

Ten new derivatives (compounds **3**, **4**, **9**, **18**, **19**, **21-25**, **Tables 1-4**) were found to be more active *in vitro* than the parent compound **1** since they were endowed with IC_{50} on CQ-R *Pf* strains lower than 100 nM. More in detail, the novel compounds **19** and **24** were identified as the best performing antiplasmodial agents on CQ-R *Pf* strains (W2) since their IC_{50}s were lower than 5 nM (**Table 4**).

SAR investigation

a) From compound 1 to 24

The structural motif of the 'eastern portion' of compound **1**, *i.e.* its (L)-leucine buthyl amide (LeuNHBut) characterized by the presence of a bulky alkyl substituent installed on an enantiomerically enriched stereogenic carbon atom and by a lipophilic buthyl-chain, was selected as the starting point of our SAR investigation (**Table 1**).

At first, compound **2**, lacking the entire LeuNHBut moiety was prepared and tested to verify the need of substituents in this 'eastern portion' of the molecule. The elimination of the eastern structural motif resulted in a complete loss of activity.

To prepare analogues with increased polarity, the buthylamide residue of the LeuNHBut moiety was then substituted with less lipophilic short-chain esters. To these means, a methyl (**3**) and an ethyl (**4**) ester derivative were synthetized. Interestingly, the IC_{50} of both compounds on CQ-R and CQ-S *Pf* strains were considerably improved (up to a 30-fold increase of potency) as well as their druggability expressed as LLE or LLE_{AT} values.

Moreover, as the presence of a stereogenic center could suggest the importance of stereoselective interactions sensitive to steric hindrance, we decided to further investigate the steric properties of methyl ester analogue **3** by synthesizing the two alanine- and isoleucine-containing derivatives **5** and **6**. The

introduction of a small alkyl chain (**6**) and of a branched one (**5**) allowed us to better understand the conformational space and freedom needed and allowed to the compounds to properly act as antiplasmodial agents. Both the new derivatives, in fact, showed an important decrease in their antiplasmodial activity, 25x and 35x, potentially ascribable to an overall change in the steric hindrance of the inserted amino acid.

In view of these results, the less lipophilic methyl ester derivative **3** was selected to continue the structure-activity investigation and structural optimization, focusing on the 'western portion' of the molecule. Thus, in the following steps, we modified only the (L)-leucine N^2,N^2-diethyl-1,2-ethylen amide of compound **3**, characterized by the presence of another sterically hindered stereogenic carbon and ethylene (C_2) alkyl linker connected a basic tertiary amine (**Table 2**).

Table 1. Structural optimization 'eastern portion' of compound **2**.

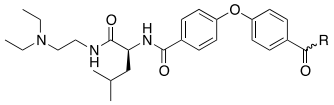

Compound	R	CQ-S D10 *Pf* strain IC_{50} (nM)	CQ-R W2 *Pf* strain IC_{50} (nM)	R.I.[a]	LLE[b]	LLE_{AT}[c]
1[8]	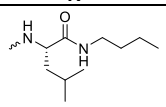	357.0±125.4	314.0±135.8	0.88	3.01	0.20
2	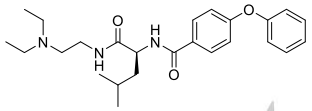	>10 μM	>10 μM	N.D.	N.D.	N.D.
3	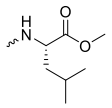	12.97±1.01	8.46±1.01	0.65	5.20	0.28
4	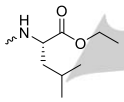	33.65±13.4	52.41±2.0	1.6	4.0	0.24
5	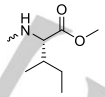	319.34±52.3	206.83±70.6	0.64	3.7	0.23
6	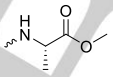	451.94±123.9	227.22±55.1	0.50	5.0	0.28
Chloroquine		20.01±5.4	360.12±41.2	18	N.D.[d]	N.D.[d]

All the data are the mean of three experiments run in duplicate. [a] Resistance Index: Ratio between IC_{50} on CQ-R and IC_{50} on CQ-S strains of *P.f*; [b] Ligand Lipophilic efficiency, defined as LLE = pIC_{50} – logP; [c] Ligand Lipophilic efficiency corrected by the number of heavy atoms; [d] Not defined

At first, we focused on the role in the antiplasmodial activity of the basic tertiary amine moiety and of the alkyl linker connecting it with the leucine residue.

Compound **7,** characterized by a longer and more lipophilic propylene (C_3) linker, was prepared and tested. Its antiplasmodial activity and also druggability (LLE) were both found to be lower than **3**; so that the SAR investigation on the 'western portion" of the molecule was continued using the shorter C_2-linker.

To investigate the connection between the nature of the tertiary amine on the antiplasmodial activity, an oxygen-containing heterocyclic amine (*i.e.* morpholine, compound **8**) and a five-membered pyrrolidine (**9**) were grafted on the C_2-linker-(L)-leucine system. While compound **8** significantly lost its antiplasmodial activity, the smaller and more lipophilic pyrrolidine derivative **9** showed an increase (2x) in its potency. Compound **10** was prepared to investigate the joined role of conformational freedom (C_2 aliphatic liker) and steric hindrance. In fact, thanks to the preparation of a N_2-methyl-N_1-(L)-leucine piperazine amide, the C_2-linker and the basic tertiary amine were combined in a single, strained and rigid six-membered heterocyclic system. This reduction of conformational freedom and the enhancement of steric hindrance resulted in a dramatic loss of potency as the IC_{50} of **10** was found to be higher than 10 μM. Our SAR investigation about the C_2 linker and the tertiary amine was finally concluded by the preparation of analogues **11**-**13** in which the C_2-linker-NR_2 moiety was removed in favor of more polar ester or amide residues. The antiplasmodial activity of the (L)-leucine methyl ester (**11**), (L)-leucine amide (**12**), (L)-lysine methyl ester (**13**), in which the basic residue was inserted in the aminoacidic side chain, were found to be dramatically decreased by the absence of the C_2-linker-NR_2 moiety.

The importance of stereochemistry and steric hindrance was then investigated. At first, the pivotal role of an enantiomerically and sterically hindered stereogenic carbon was confirmed by the preparation of the N^2,N^2-diethyl-ethylen (**14**) and of the 2-(pyrrolidin-1-yl)ethylen amide derivatives **14** and **15** in which the C_2-linker-NR_2 moiety was directly coupled with the 4,4'-bisbenzoic acid core. Interestingly, while compound **14** suffered a dramatic decrease of its antiplasmodial activity (IC_{50} > 10 μM). The 2-(pyrrolidin-1-yl)ethylen amide derivative **15** maintained a good inhibitory activity on CQ-R *Pf* strains (*ca* 0.4 μM)

suggesting a crucial role of the pyrrolidine residue whose pharmacophoric role appeared particularly relevant toward resistant *Pf* strains according to its pretty low RI (0.21). Moreover, the bioactivity of both compounds **14** and **15** highlighted the possible pivotal role of the amide system (C=O-NH) of the aminoacid residue of the eastern portion as it could be involved in the formation of hydrogen bonds. The presence of stereoselective interactions between **3** and its postulated target was further suggested by the significant reduction of potency of the (R)-leucine derivative **16**. Consequently, the role of the steric hindrance of the (*S*)-configured amino acid residue, was investigated by synthesizing the (S)-alanine and (S)-isoleucine-containing derivatives **17** and **18**.

Remarkably, the antiplasmodial activity of **17**, was significantly reduced by the introduction of a small alkyl chain while the potency of **18** containing a sterically demanding and lipophilic isoleucine, was comparable to that of compound **3** and further improved by the introduction of the pyrrolidine residue in place of the original diethylamine (compound **19**).

Table 2. Structural optimization 'western portion' of compound **2**.

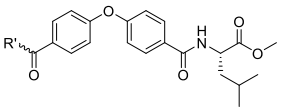

Compound	R'	CQ-S D10 *Pf* strain IC_{50} (nM)	CQ-R W2 *Pf* strain IC_{50} (nM)	R.I.[a]	LLE[b]	LLE_{AT}[c]
7	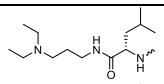	219.34±74.4	101.37±30.9	0.46	4.82	0.26
8	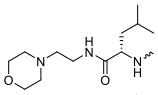	1150.6±242.1	1114.72±355.1	0.96	2.38	0.19
9	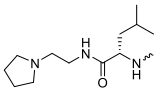	5.13±1.7	4.01±1.2	0.78	5.22	0.28
10	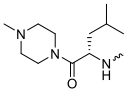	>10000	> 10000	N.D.	1.26	0.15
11	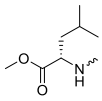	>9000	> 9000	N.D.	0.53	0.13
12	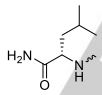	5072.9±1078.4	3366.33±1228.8	0.66	1.91	0.18
13	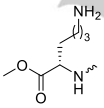	7846.5±1624.3	8338.31±2933.9	1.06	4.55	0.28
14	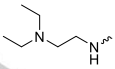	>10000	> 10000	N.D.	2.85	0.22
15	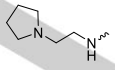	1814±687.3	390.37±126.6	0.21	3.91	0.26
16	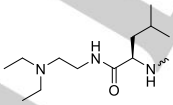	2967.4±598.2	1140.56±335.1	0.38	3.07	0.28
17	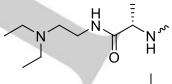	2270.2±235.1	1234.60±417.6	0.54	5.38	0.30
18	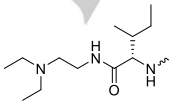	5.83±2.0	2.48±0.8	0.42	5.66	0.29
19	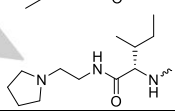	0.488±0.151	0.34±0.122	0.70	6.21	0.31

All the data are the mean of three experiments run in duplicate. [a] Resistance Index: Ratio between IC_{50} on CQ-R and IC_{50} on CQ-S strains of *P.f*; [b] Ligand Lipophilic efficiency, defined as LLE = pIC_{50} – logP; [c] Ligand Lipophilic efficiency corrected by the number of heavy atoms;

Table 3. Structural optimization 'eastern portion' of compounds **1**, **18** and **19**.

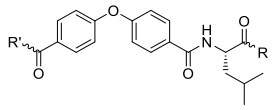

Compound	R'	R	CQ-S D10 *Pf* strain IC_{50} (nM)	CQ-R W2 *Pf* strain IC_{50} (nM)	R.I.[a]	LLE[b]	LLE_{AT}[c]
20	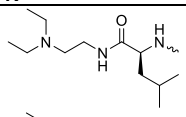	OH	244.42±65.4	154.64±37.9	0.63	5.2	0.28
21	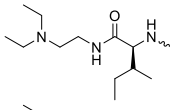	NHBut	68.41±25.1	80.05±18.8	1.17	3.60	0.22
22	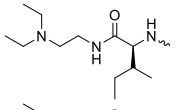	NHMe	118.34±38.6	70.26±20.1	0.59	4.90	0.27
23	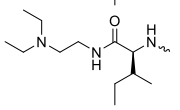	NH_2	4.85±6.3	3.23±1.9	0.66	6.50	0.32
24	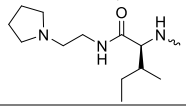	NH_2	2.45±0.85	3.13±0.60	1.27	6.20	0.31

All the data are the mean of three experiments run in duplicate. [a] Resistance Index: Ratio between IC_{50} on CQ-R and IC_{50} on CQ-S strains of *P.f*; [b] Ligand Lipophilic efficiency, defined as LLE = pIC_{50} – logP; [c] Ligand Lipophilic efficiency corrected by the number of heavy atoms;

Analogue **19** summarizes all the beneficial structural features discovered in these two rounds of SAR investigation: it possesses a reduced lipophilic character and present the proper steric hindrance and configuration coupled with the best performing C_2-linker-NR_2 system.

Accordingly, its antiplasmodial activity was less than 1 nM on both CQ-S and CQ-R *Pf* strains and its LLE was mostly doubled. Considering the narrow structure-activity relationships observed, we focused our attention only on the hydrolysable (L)-leucine methyl ester moiety (LeuOMe) of compounds **18** and **19** (**Table 3**). In fact, the preparation of the free acid form of compound **3**, analogue **20**, demonstrated the key role of its LeuOMe residue: the antiplasmodial activity of **20** was about 200-times lower than **3**. Based on these considerations, our choice was to substitute the labile methyl ester bond with a more robust amide linkage to improve its hydrolytic stability while preserving its proper balanced characteristics of polarity and lipophilicity.

Three amide derivatives, with different polarities, were prepared: the buthyl amide **21**, the methyl amide **22** and the primary amide **23**. Compound **23** was the only compound of this series that retained the original antiplasmodial activity while boosting its chemical stability and druggability.

In the view of all the collected SAR information, compound **24**, in which the (L)-leucine amide was inserted into a molecular skeleton containing the 4,4'-oxybisbenzoyl amide core connected to the two 'optimized' eastern and western portions, was eventually prepared and assessed as the best antiplasmodial agent of the series (LLE: 6.20; IC_{50} (CQ-R, W2) = 3.13 nM; IC_{50} (CQ-S, D10) = 2.45 nM).

b) What have we learnt?

Since both compounds **19** and **24**, the two most potent analogues of the series, do not present any known and common antimalarial pharmacophoric groups, it is likely that these molecules owe their activity to a new mechanism of action by the interaction, with a (novel) biological target that still remains unknown. However, the SAR studies conducted during the structural optimization of compound **1** allowed us to gain lots of information about the characteristic of a hypothetical binding pocket and modes of interaction between these oxybisbenzoylamides-based scaffolds and their postulated target. Thus, we were able to draw a qualitative description of the streoelectronic, conformational and polarity features needed to promote a proper binding of **24** to its (still unknown) biological target (**Figure 2**). Generally speaking, a complex equilibrium of conformational freedom and restrains seems to be needed to properly arrange the structure of **24** in what appears as a highly stereoselective and stereosensitive binding pocket. The presence of the highly rotatable 4,4'-oxybisbenzoic acid core seems crucial in this context allowing the bulky nonpolar alkyl substituents of both the leucine and isoleucine residues of **24** to be properly placed in a large enough lipophilic pocket, orientating, accordingly, the Lewis acid and basic groups (CO and NH). It can be also argued that the hypothetical binding site of biological target of compound **24** could be characterized by the presence of a framework of polar and lipophilic regions and hydrogen bonding residues (as the C=O-NH systems depicted in black in **Figure 2**) which delineates a narrow and specific pattern of interactions highly stereoselective and sensitive to steric hindrance. It's noteworthy how "small" modifications in the chemical structure of the C_2-linker-NR_2 system of the 'western portion' appeared to highly modulate the antiplasmodial activity of the resulting compounds.

In order to verify our hypotheses and gain a clearer description of the SAR summarized in **Figure 2**, a new set of compounds was synthetized (**Table 4**).

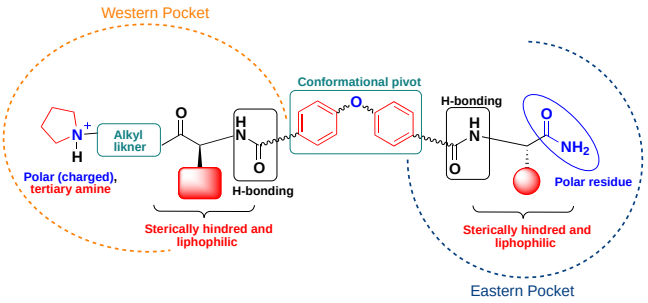

Figure 2. Schematic representation of the streoelectronic, conformational and polarity features of **24**.

At first, we wanted to demonstrate that the 4,4'-oxybisbenzoic acid core acts as a privileged scaffold for these family of compounds, thanks to its peculiar conformational features connected with the presence of a diaryl ether linkage. Consequently, it was substituted with groups characterized by different degrees of conformational freedom: a highly-rotatable methylene bond (compound **25**), a more rigid sulfone linkage (**26**) and a planar and unbending furan ring (compound **27**). The antiplasmodial activity of the highly-rotatable, tetrahedral-shaped methylene analogue **25** on CQ-R *Pf* strains was found to be just slightly reduced when compared to the parental compound **3**; but, the antiplasmodial activities of the more conformationally restrained analogues **26** and **27** were significantly reduced. As expected, the 4,4'-oxybisbenzoic acid core confirmed its pivotal role as 'conformational pivot' for the molecule to assume a proper 3D-shape promoting the interaction with the biological target. Furthermore, the oxygen atom of the diaryl ether could play an important role in the binding event, maybe due to desolvation energy gains and/or H-bonding *via* its free electron pairs.

Moreover, as it was easily predictable by their different shapes, the insertion of a SO_2 or a furan group in place of an oxygen could harm the bioactivity also by modifying the distances and the geometries of interaction between the different pharmacophoric groups and their target.

Table 4. SAR investigation: "conformational pivot" and basic heads **2**.

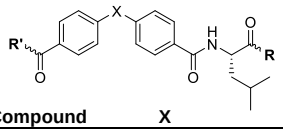

Compound	X	R'	R	CQ-S D10 *Pf* strain IC_{50} (nM)	CQ-R W2 *Pf* strain IC_{50} (nM)	R.I.[a]	LLE[b]	LLE_{AT}[c]
25	CH_2	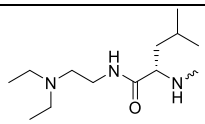	OMe	116.61±8.34	51.10±18.1	0.43	3.83	0.23
26	SO_2	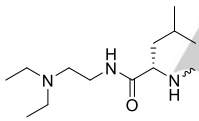	OMe	4524.34±1963.4	2601.56±918.1	0.58	3.91	0.26
27	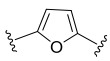	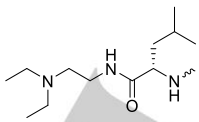	OMe	670.71±134.5	368.74±15.5	0.54	4.45	0.25
28	O	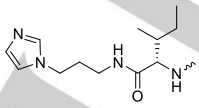	NH_2	1403.78±138.6	1126.34±16.4	0.80	3.14	0.21
29	O	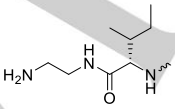	NH_2	203.36±20.9	329.91±16.5	1.62	6.10	0.33
30	O	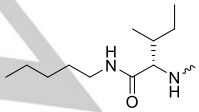	NH_2	1532.70±381.8	2695.87±842.5	1.75	1.33	0.16
31	O	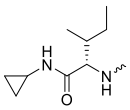	NH_2	4987.45±1321.7	6119.31±2060.3	1.22	1.83	0.18

All the data are the mean of three experiments run in duplicate. [a] Resistance Index: Ratio between IC_{50} on CQ-R and IC_{50} on CQ-S strains of *P.f*; [b] Ligand Lipophilic efficiency, defined as LLE = pIC_{50} – logP; [c] Ligand Lipophilic efficiency corrected by the number of heavy atoms; [

Since specific steric and polar features seems to be crucial for a proper interaction of the 'western portion' of this family of compounds with their biological target (the insertion of an additional methylene group in the alkyl-linker chain of compound **3** remarkably reduced its antiplasmodial activity), we decided to further stress the nature of the optimal features of the C_2-linker-NR_2 system. Moreover, a key role of steric hindrance and conformational freedom was previously suggested by the low antiplasmodial potency ($AvIC_{50}$ > 10 μM) of compound **10** in which the C_2-linker-NR_2 system is locked in a rigid cyclic system (**Table 2**).

To further confirm the narrow SAR observed, compounds **28**-**31**, containing variations in the polarity and steric hindrance of the C_2-linker-NR_2 system were prepared and tested. (**Table 4**).

As hypothesized, the potency of compounds **28**-**31** were considerably reduced. Attesting the importance of a proper balancing between the polar and the lipophilic character of the C_2-linker-NR_2 system, the introduction of a basic aromatic heterocycle (compound **28**) or the insertion of a C3-spaced, polar and highly hydrophilic primary amine (compound **29**) resulted in a significant reduction of antiplasmodial activity, especially in the case of compound **28**. Moreover, the elimination of the basic -NR_2 moiety (compounds **30** and **31**) resulted in a dramatic decrease in antiplasmodial potency when compared to **24**.

c) *In Silico* Pharmacophore Mapping

The qualitative description of narrow SAR at the basis of **24** antiplasmodial activity described in **Figure 2** encouraged us to further investigate its pharmacophore.

The CCDC suite was used to generate a pharmacophore model by superposing a set of active molecules assuming binding to the same target with the same binding mode.[14,15] Details are described in the experimental and briefly described below.

In order to build the pharmacophore model, a cluster of active compounds was identified selecting each member on the basis of its average antiplasmodial activity (arithmetic mean of the IC50 on W2 and D10 *P.f.* strains) on the two tested *Pf* strains expressed as the arithmetic media of the corresponding IC_{50} ($AvIC_{50}$ < 100 nM; **3**, **4**, **9**, **18**, **19**, **21**-**25**). Consequently 200 conformers were generated for each compound, using the Mercury module of the CCDC suite. The Hermes module was then used to generate eight different overlays describing a hypothetical pharmacophore model. The lowest in energy and most statistically relevant (on the basis of their calculated internal energy and statistical score) was selected (**Figure 3**).

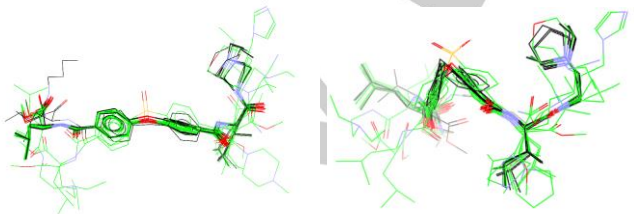

Figure 3. Ligand overlay of the 10 active molecules (black) and the 14 decoy molecules (green).

The chosen model was, at first, visualized showing the H-bond interactions as vectors and the lipophilic interactions as dots (**Figure 4**). As can be seen, in the selected overlay all the 10 active molecules are successfully arranged with the same spatial orientation, placing large alkyl substituents toward the same direction and over imposing the pivotal donor/acceptor groups (*e.g.* the basic tertiary amine residue or the carbonyl groups).

To verify this pharmacophore model, 14 decoy molecules ($AvIC_{50}$ > 1μM; compounds **2**, **8**, **10**-**17**, **26**-**28**, **30**-**31**, **Table S1** in **Supplementary Information**) were considered. The decoys were added to the selected model and a new overlay was calculated. As shown in **Figure 3**, the 14 decoy molecules (green) hardly fit the calculated pharmacophore model (black). Additionally, a score was calculated for each compound of the overlay and reported in **Table S1**.

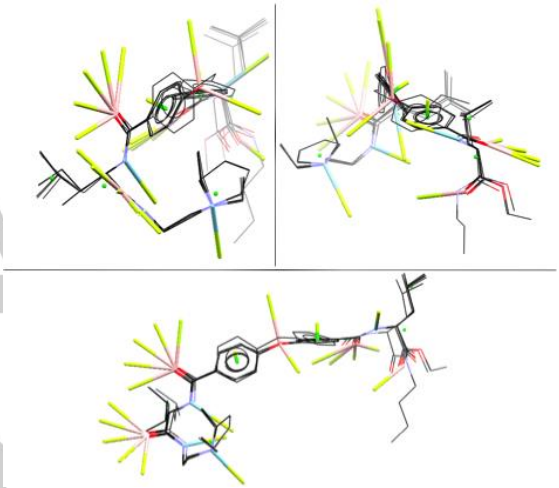

Figure 4. A "*vector and dot*" representation of the calculated pharmacophore model.

Using the score of the most potent compound **19** ($AvIC_{50}$ < 0.5 nM), normalized scores were also calculated: 9 of the 10 active compounds ($AvIC_{50}$ < 100 nM) were found to be higher than 0.9. In order to better visualize these results, the normalized scores were charted against the average of the IC_{50}s (**Chart A**): the orange dots are associated with the decoys molecules, the green with the active compounds. As can be seen, our *in silico* model was able to successfully distinguish between the most and the less active compounds, the only exceptions being the 'truncated' compound **2** and the methylenedibenzoic acid-derivative **25**. Compound **2**, even if inactive ($AvIC_{50}$ > 1250 nM), was easily overlayed by the CCDC suite within the pharmacophore given its simplified structure resulting in a score of 0.88, while **25** ($AvIC_{50}$ = 83.85 nM) was wrongly labeled as a decoy molecule (normalized score = 0.74) due to the lack of the oxybisbenzoic acid core, which dramatically affected its calculated overlay score.

Furthermore, we further validated our *in silico* model by repeating the entire process excluding **24** from the generation of the pharmacophore model and, then, considering it as a 'decoy-probe' in a second overlay experiment. The obtained normalized scores were, again, charted against the $AvIC_{50}$s (**Chart B**). As it

shown in **Chart B**, **24** (the blue triangle) was correctly placed inside the area of the active compounds, even if it was excluded by the cluster of active compounds (AvIC_{50} < 100 nM) used to generate the pharmacophore. The methylenedibenzoic acid-derivative **25** was found, again, as the only out-layer of the series.

Finally, a surface describing the donor (blue), acceptor (red) and non-polar (orange) interactions was generated on the base of the 'vector and dot' representation reported in **Figure 4** to broaden the visualization our pharmacophore model (**Figure 6**).

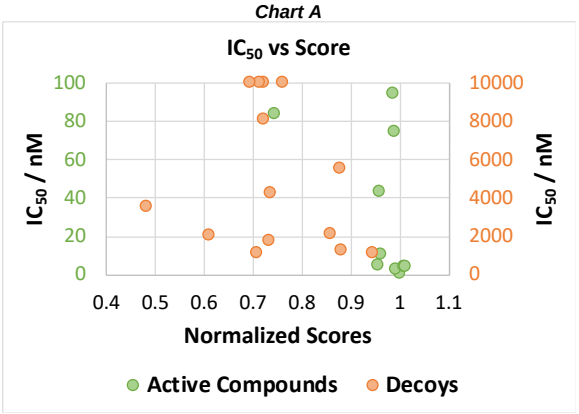

Figure 5. ***Chart A***) Scattered representation of the average IC_{50} of the active (green) and decoy (orange) compounds against their normalized scores; ***Chart B***) Scattered representation of the average IC_{50} of the active compounds (green) and **24**-probe (blue) against their normalized scores.

Compound 24: biological profile

Given its promising antiplasmodial activity and the improvements in its druglikeness, here described with the calculation of the two parameters LLE and LLE_{AT}, the biological profile of the novel compound **24**, was preliminarily evaluated in terms of selectivity of action and metabolic stability.

Accordingly, the *in vitro* selectivity index of **24** (IVSI) was calculated and compared with its methyl ester analogue **19**. A human microvascular endothelial cell line (HMEC-1) was used to test the cytotoxicity of the two compounds. Obtained results are summarized in **Table 5**. Both **19** and **24** showed considerably higher IVSI than the parent compound **1**.[8] Interestingly, the IVSI of **24** was found to be higher than dihydroartemisinin (DHA), equally potent but more cytotoxic than **24** *in vitro*.

Furthermore, water solubility and metabolic stability of **24**, were also tested. At pH 3.0 and 7.4, **24** solubility resulted 220 μM and 190 μM, respectively. Moreover, it demonstrated to be stable in water (pH 7.4) for 3 hours as the 95% of it was recovered after the incubation (**Table 6**).

Interestingly, its metabolic stability was found to be poor. Along with a high microsomial intrinsic clearance (286 μL min^{-1} mg^{-1} in human microsomes), the remaining percentage of **24** was only 14% after 30 minutes. Furthermore, this chemical showed a low intestinal absorption and a low P-glycoprotrein (Pgp) binding. In fact, as shown in **Table 6**, **24** absorption did not change whether or not Pgp was inhibited: the efflux and the absorption were found to be the same in both cases (5.2 vs 5.96 and 0.61 vs 0.89, respectively). As can be easily imagined, the low metabolic stability affecting **24** might be due to the fact that the molecule is still a peptide, a well-known target of metabolic enzymes, and also contains easily-oxidizable moiety such as the five-member ring of pyrrolidine. Moreover, the presence of 15 rotatable bonds might impair its intestinal absorption.

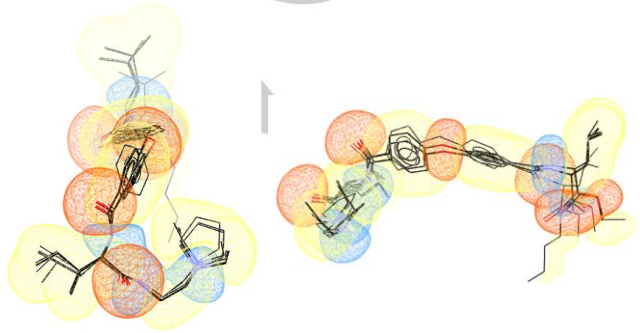

Figure 6. A force-field representation of the calculated pharmacophore model: the areas of donor, acceptor and non-polar interaction are highlighted in blue, red and yellow, respectively.

Furthermore, water solubility and metabolic stability of **24**, were also tested. At pH 3.0 and 7.4, **24** solubility resulted 220 μM and 190 μM, respectively. Moreover, it demonstrated to be stable in water (pH 7.4) for 3 hours as the 95% of it was recovered after the incubation (**Table 6**).

Interestingly, its metabolic stability was found to be poor. Along with a high microsomial intrinsic clearance (286 μL min^{-1} mg^{-1} in human microsomes), the remaining percentage of **24** was only 14% after 30 minutes. Furthermore, this chemical showed a low intestinal absorption and a low P-glycoprotrein (Pgp) binding. In fact, as shown in **Table 6**, **24** absorption did not change whether or not Pgp was inhibited: the efflux and the absorption were found to be the same in both cases (5.2 vs 5.96 and 0.61 vs 0.89, respectively). As can be easily imagined, the low metabolic stability affecting **24** might be due to the fact that the molecule is still a peptide, a well-known target of metabolic enzymes, and also contains easily-oxidizable moiety such as the five-member ring of pyrrolidine. Moreover, the presence of 15 rotatable bonds might impair its intestinal absorption.

Conclusions

In this work we have conducted a detailed SAR investigation about the chemical and conformational features of the 4,4'-oxybisbenzoyl amide core identified as the pharmacophore of

the potent antiplasmodial agent previously described by us (compound **1**, **Figure 1**).[8]
Thanks to the high number of structurally-simplified analogues of **1** synthetized during this study, we could successfully optimize its chemical structure affording a more potent, selective, low nanomolar inhibitor of *Pf* growth free from cross resistance (**24**) whose performances resulted comparable with known antimalarial drugs (**Table 6**).

Table 5. Comparison between the IVSI of compounds **1**, **19** and **24** and the two reference drugs chloroquine and dihydroartemisinin.

Compound	Structure	CQ-R W2 *Pf* strain IC_{50} (nM)	Cytotoxicity: HMEC-1[a] IC_{50} (nM)	IVSI[b]
1	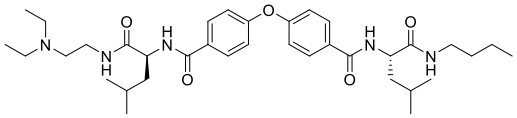	314.0±135.8	17000	54
19	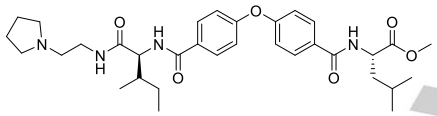	0.34±0.122	23000	70000
24	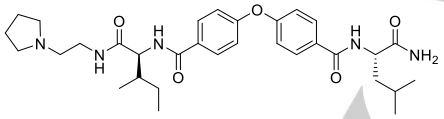	3.13±0.60	> 25000	> 7950
Chloroquine (CQ)	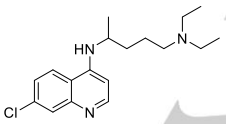	430.30±143.3	> 25000	> 58
Dihydroartemisinin (DHA)	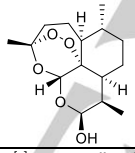	3.32±0.10	5800	1750

All the data are the mean of two experiments run in duplicate. [a] Immortalized human microvascular endothelial cell line; [b] *In vitro* selectivity index, defined as: $IC_{50}^{HMEC-1}/IC_{50}^{W2\ Pf\ strain}$.

Table 6. Stability profiles of **24**.

Sol[a] (µM)		Plasma Stab[b] (%)	Met Stab[c] (%)	MDCK - MDR1		Microsomial Intrinsic Clearance[f] (µL/min/mg)		
pH 3.0	*pH 7.4*	*Rat*	*Remaining*	P_{app} AB[d] (10^{-6} cm/s)	*Efflux Ratio*[e]	*Clint HLM*	*Clint mRLM*	*Clint mMLM*
220	190	95	28	0.24	1.7	85.50	>700	>700

[a] Solubilities were determined at pH 7.4 at pseudothermodynamic equilibrium.
[b] Plasma stability was determined as percentage remaining after incubation for 3h with fresh rat plasma.
[c] Metabolic stability was determined as percentage remaining after incubation for 1 h with recombinant hCYP3A4.
[d] MS-based quantification of apical / basolateral transfer rate at 2 mM across contiguous monolayers of MDCK cells.
[e] Ratio of (basal / apical) to (apical / basal) transfer rate at 2 mM across contiguous monolayers of MDCK (MadineDarby canine kidney) cells.
[f] Predicted hepatic clearance from human, rat and mouse liver microsomal stability assay.
See **Experimental Section** for further details on all assays.[16,17]

The collected data allowed us to delineate the narrow structure-activity connections characterizing the molecular skeleton of **24** and of the related compounds **19**, **22** and **23** (**Figure 2**).
Since to the best of our knowledge, **24** potency as *Pf* growth inhibitor cannot be ascribed to any of the established and characterized antiplasmodial pharmacophores, we also conducted an *in silico* pharmacophore modeling to gain additional information about this potent class of the 4,4'-oxybisbenzoyl amide-based compounds. The ligand overlay experiment (**Figure 3**) and the consequent pharmacophore mapping (**Figures 4** and **6**) further confirmed the very narrow SAR discovered during the structural optimization campaign and highlighted a specific pattern of stereoselective, polar and H-bonding connections likely involved in the interaction with a (still unidentified) protein target.
The druggability of compound **1**, was also investigated and improved during this study introducing modifications driven by the corresponding values of LLE and LLE_{AT} thus significantly improving these parameters (**Figure 7**).
Finally, the metabolic and chemical stability profiles of compound **24** were preliminary investigated, underlining some critical issues connected to its bioavailability which will be the

focus of another structural optimization campaign conducted, this time, on the basis of the predictive pharmacophore model we build from our *in silico* investigations (**Charts A** and **B**).

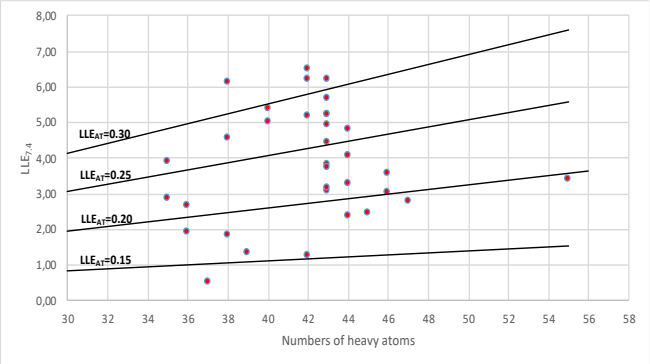

Figure 7. LLE_{AT} distribution for all the synthetized compounds.

Experimental Section

a) Chemistry

Materials and methods

All commercially available solvents and reagents were used without further purification, unless otherwise stated.

NMR spectra were recorded on a Varian Mercury 300 VX spectrometer in $CDCl_3$, CD_3OD or DMSO-d6 and chemical shifts were reported in ppm (δ). Peaks were assigned with 2D COSY experiments and are in agreement with the proposed structures.

TLC was carried out on Merck precoated 60 F254 plates using UV light and dipping with ethanol/phosphomolybdic acid 10% or a 10% w/v ethanolic solution of ninidrine.

Flash column chromatography was performed using silica gel 60 (0.040-0.063 mm, Merck).

Organic phases were dried over anhydrous sodium sulphate. Concentrations were performed under diminished pressure (1-2 kPa) at a bath temperature of 40 °C.

ESI – HRMS were recorded on a ICR-FTMS APEX II (Bruker Daltonics) mass spectrometer.

Preparative HPLC purifications were performed using CH_3CN/H_2O + CF_3COOH gradient and a Waters 2525 Binary Gradient Module equipped with a Agilent Zorbax SB-C18 column.

Purities of final compounds were determined by HPLC using CH_3CN/H_2O + CF_3COOH gradient and a Purospher RP18 5 µm column on a Hitachi Elite Lachrom Instrument equipped with a DAD detector.

General procedure A: synthesis of non-commercially available amines

The selected *N*-protected aminoacid (1.1 eq) and primary amine (1.0 eq) were dissolved in DCM (5 mL $mmol_{amine}^{-1}$), the resulting solution was cooled at 0 °C and TBTU was added (1.1 eq); pH was set at 8 by adding NMM and the reaction was stirred at room temperature overnight. After that, the mixture was washed three times with a saturated aqueous solution of $NaHCO_3$, two times with water and brine and finally dried over Na_2SO_4 and concentrated again in *vacuo*. The crude product was purified by flash column chromatography on silica gel suing a gradient of MeOH in DCM as mobile phase affording the desired *N*-protected amines (**a-m**).

General procedure B: the deprotection of N-Boc amines

The *N*-Boc amine were dissolved in a dioxane solution of HCl (2 M) and stirred at room temperature for 3 hours. After that, the solvent was removed by in *vacuo* concentration affording the corresponding primary amine which was used without any further purification.

General procedure C: deprotection of N-Cbz amines

The *N*-Cbz amine was dissolved in MeOH (10 mL $mmol_{amime}^{-1}$), Pd/C was added (8 mg mL_{MeOH}^{-1}) and the mixture was stirred at room temperature in hydrogen atmosphere for 3-6 hours. After that, the catalyst was removed by filtration and the solvent concentrated in *vacuo* affording the desired amine used without any further purification.

General procedure D: synthesis of compounds 3-19 and 21-31

1g of 4,4'-oxybisbenzoic acid (3.87 mmol, 1.1 eq) and the proper amount of a selected amine (3.51 mmol, 1.0 eq) were dissolved in 250 mL of dry DMF. 1.25 g of TBTU (3.87 mmol, 1.1 eq) were then added to the previously mentioned solution which was ice-cooled at 0 °C; pH was set at 8 by adding NMM. The reaction was stirred at room temperature overnight.

After that, DMF was removed *in vacuo*, the residue was taken up in AcOEt (250 mL), washed with water (150 mL, 2x), brine (150 mL), dried over Na_2SO_4 and concentrated again in *vacuo*.

The obtained residue was dissolved again in 250 mL of dry DMF and subjected to a second coupling reaction with a different primary amine following the procedure decried above.

At the end of this second coupling, DMF was removed again *in vacuo* and the resulting residue was taken up in 150 mL of DMC, washed a saturated aqueous solution of $NaHCO_3$ (150 mL) and brine (150 mL). Combined organic layers were dried over Na_2SO_4 and concentrated again in *vacuo* affording a crude mixture of coupled products.

Finally, target compounds were isolated and purified by RP preparative HPLC and converted into the corresponding hydrochloride salts using a 1M aqueous solution of hydrochloric acid.

Yields were calculated with the respect of the amount of acid reacted in the first coupling.

For the synthesis of compounds **25**, **26** and **27** 1g of 4,4'-methylenedibenzoic (3.26 mmol), 4,4'-sulfonyldibenzoic (3.90 mmol) and 4,4'-(furan-2,5-diyl)bisbenzoic acid (3.24 mmol) was used, respectively, and the amount of TBTU and primary amines calculated accordingly.

For the experimental details about the preparation of amines (**a-m**) and compounds **2-31** see **Supplementary Information**.

b) Biology

P. falciparum cultures and drug susceptibility assay

Plasmodium falciparum cultures were carried out according to Trager and Jensen with slight modifications.[20] The CQ-susceptible strain D10 and the CQ-resistant strain W2 were maintained at 5% hematocrit (human type A-positive red blood cells) in RPMI 1640 (EuroClone, Celbio) medium with the addition of 1% AlbuMax (Invitrogen, Milan, Italy), 0.01% hypoxanthine, 20 mM Hepes, and 2 mM glutamine. All the cultures were maintained at 37 °C in a standard gas mixture consisting of 1% O_2, 5% CO_2, and 94% N_2. Compounds were dissolved in DMSO and then diluted with medium to achieve the required concentrations (final DMSO concentration <1%, which is non-toxic to the parasite). Drugs were placed in 96-well flat-bottomed microplates and serial dilutions made. Asynchronous cultures with parasitaemia of 1-1.5% and 1% final hematocrit were aliquoted into the plates and incubated for 72 h at 37 °C. Parasite growth was determined spectrophotometrically (OD_{650}) by measuring the activity of the parasite lactate dehydrogenase (pLDH), according to a modified version of the method of Makler in control and drug-treated cultures.[13] The antimalarial activity is expressed as 50% inhibitory concentrations (IC_{50}); each IC_{50} value is the mean and standard deviation of at least three separate experiments performed in duplicate.

Cytotoxicity assays

Cytotoxicity was evaluated on a long-term cell line of human dermal microvascular endothelial cells (HMEC-1) immortalized by simian virus 40 (SV40) large T antigen. HMEC-1 were maintained in MCDB 131 medium (Gibco-BRL, Paisley, Scotland) supplemented with 10% fetal calf serum (HyClone, Logan, UT, USA), 10 ng/ml epidermal growth factor (PeproTech, Rocky Hill, NY, USA), 1 µg/ml hydrocortisone (Sigma Italia, Milan, Italy), 2 mM glutamine (EuroClone, Pero, Italy) and 20 mM HEPES buffer (pH 7.3) (EuroClone).

For the cytotoxicity assay, cells were seeded in 96 well flat bottom tissue culture clusters (Costar, NY, USA) at 10^4 cells/well, after 24h cells were treated with serial dilutions of test compounds in a final volume of 200 µl/well for 72 h. The 3-(4,5-dimethyl-2-thiazolyl)- 2,5-diphenyl-2H tetrazolium bromide (MTT) (Sigma) cytotoxicity assay was used to measure cell viability, as described elsewhere. Cytotoxicity was expressed as the 50% inhibitory concentration (IC_{50}).

Solubility assay

Standard and sample solutions were prepared from a 10 mM DMSO stock solution using an automated dilution procedure. For each compound, three solutions were prepared; one to be used as standard and the other two as test solutions. Standard: 250 µM standard solution in acetonitrile/ buffer, with a final DMSO content of 2.5% (v/v). Test sample for pH 3.0: 250 µM sample solution in acetic acid 50 mM, pH =3, with a final DMSO content of 2.5% (v/v). Test sample for pH 7.4: a 250 µM sample solution in ammonium acetate buffer 50 mM, pH = 7.4, with a final DMSO content of 2.5% (v/v). The 250 µM product suspensions/solutions in the aqueous buffers were prepared directly in

Millipore MultiScreen-96 filter plates (0.4 µm PTCE membrane) and sealed. Plates were left for 24 h at room temperature under orbital shaking to achieve "pseudo-thermodynamic equilibrium" and to presaturate the membrane filter. Product suspensions/solutions were then filtered using centrifugation, diluted 1:2 with the same buffer solution, and analyzed by UPLC/UV/TOF-MS, using UV detection at 254 nm for quantitation. Solubility was calculated by comparing the sample and standard UV areas: S = (Asmp x FD x Cst)/Ast, where S was the solubility of the compound (µM), Asmp was the UV area of the sample solution, FD was the dilution factor (2), Cst was the standard concentration (250 µM), and Ast was the UV area of the standard solution.

Plasma stability

Fresh plasma spiked with a 250 µM solution of test item dissolved in acetonitrile 12%, were divided in 3 aliquots (one for each time point) in a 96-well plate (in duplicate) and incubated at 37 °C under gentle agitation for up to 3 h. At time 0 and afterwards at the prefixed time points of 30 min and 3 h, two aliquots were transferred, and 3 volumes of acetonitrile were added for protein precipitation, followed by centrifugation (4000 rpm, 15 min, 4 °C) and dilution with 0.1% HCOOH. Analysis by LC-ESI+-MSMS using a fast gradient were performed using an API4000 triple quadrupole mass spectrometer (Applied Biosystems) in the multiple reaction monitoring mode (MRM). Results, as average of two replicates, were obtained by comparing the peak area at the different time points (30 min and 3 h) with that at time 0 and were reported as percentage remaining: Percent remaining = Area STM/Area time 0 × 100. Compounds were defined as stable, moderately unstable, or unstable based on the Percent Remaining: 80–100 stable, 50–80 moderately unstable, <50 unstable.

Metabolic stability assay

Compounds in 10 mM DMSO solution were added to an incubation mixture in a 96-well microplate containing 20 pmol/mL of hCYP3A4 (0.1-0.2 mg/mL protein). The mixture was split in two aliquots: one receiving a NADPH regenerating system, the other an equal amount of phosphate buffer. The final substrate concentration was 1 µM along with 0.25% of organic solvent. Incubation proceeded for 1 h at 37 °C and was stopped by addition of acetonitrile to precipitate proteins. Metabolic stability was given as the percent remaining following incubation with cofactor (NADPH) with reference to the incubation mixture without NADPH: % remaining = Area NADPH x 100/Area ctrl where Area ctrl was the MS peak area of the sample solution without NADPH and Area NADPH was the MS area of the sample solution with NADPH. The % CV obtained was typically within 10%.

MDCK cellular permeability

Madin–Darby Canine Kidney were maintained in tissue culture flasks in EMEM with Glutamax added with 1% MEM, Penicillin (100 U/ml), Streptomycin (100 µg/ml), 10% FBS. Five days before the permeability experiment, the cells were split and placed on permeable cell culture inserts (24-well Millipore) at a density of 25,0000 cells/well. Transepithelial electrical resistance (TEER) was measured for each well before incubation using an EVOMX instrument (WPI) to ensure that the monolayer was confluent and the tight junctions intact. A TEER >70 Ohm × cm2 was considered suitable for experimentation. Compounds (10 µM in HBSS-Hepes buffer) were added in duplicate to the donor chamber and buffer to the acceptor chamber (alternatively apical and basolateral) and incubated for 2 h at 37 °C under gentle agitation. Standards with a high (antipyrin), low (cimetidine) and medium (warfarin) permeability were incubated in the same plate under the same conditions. An aliquot (100 µL) from each well (both apical and basolateral) at time 0 and 120 min was filtered and analysed by UPLC/TOF-MS. Following incubation, the cell monolayer was washed and incubated with Lucifer Yellow, a fluorescent probe with low permeability, to verify monolayer integrity after incubation. The UPLC separation was performed using a C-18 column (Acquity UPLC BEH C18, 1.7 µm, 2.1 × 50 mm, Waters). Samples were analysed using an LTC premier TOF (Waters). The ESI positive W mode scan type was applied and the Total Ion Current (TIC) scan range extended from 100 to 800 amu, with a scan time of 0.08 s. Acquisition was from 0.3 to 1.8 min. Quantitative data were automatically produced using the OpenLynx software. The apparent permeability (Papp) in cm/sec was calculated using the following equation in both directions (apical-to-basolateral and basolateral-to-apical): Papp = dC × Vr/dt × A × C0 (where Vr was the volume (mL) of the receiver chamber, A was the surface area of the cell culture insert and dt was the time in sec) Mass balance in both directions was estimated by the following equation: Mass balance = (Final Donor Mass + Mass Transferred)/Initial Donor Mass. The efflux ratio was calculated by comparing Papp B→A with Papp A→B. A high efflux ratio was an indication of the compound being a substrate for efflux transporters. The alert threshold was an efflux ratio >3.

Microsomial intrinsic clearance

Test compound was incubated at 1 µM concentration in 100 mM phosphate buffer (pH 7.4) and 1 mM EDTA with 0.2 mg/mL human or mouse or rat hepatic microsomal protein. The enzymatic reaction was initiated by addition of a NADPH regenerating system (final concentrations: 2 mM ß-nicotinamide adenine dinucleotide phosphate (NADP) + 10 mM glucose-6-phosphate (G6P) + 0.4 U/mL glucose-6-phosphate dehydrogenase (G6PDH)). Reactions were terminated at regular time intervals (0–5–10–20–40 min) by adding an equal volume of acetonitrile. All incubations were performed in duplicate. Verapamil as positive control for the assay was incubated in parallel under the same conditions. Samples were analyzed by UPLC/TOF-MS. Calculation Substrate depletion data (peak area at different time points) were fitted to a monoexponential decay model (eq 1), with a 1/y weighting, C(t) = C0e–kt, where C0 was the substrate concentration in the incubation media at time 0 and k was the terminal rate constant. Under the assumption that the concentration of 1 µM was far below the Km of the test compound, the in vitro Clint was calculated by dividing the elimination constant (K) for the microsomal protein concentration (PMS), expressed in mg/µL, to obtain Clint in units of µL/min/mg protein: Clint = K/PMS = µL/min/mg protein. Compounds were defined as low, medium, or highly metabolized based on the in vitro Clint values: <3.4, low; 3.4–92.4, medium; >92.4, high.

c) Ligand overlay and pharmacophore generation

The CCDC-suite (https://www.ccdc.cam.ac.uk/) was used to generate a 2D-pharmacophore based on the ligand overlay of the active compounds (**3**, **4**, **9**, **18**-**25** average IC_{50} < 100 nM). At first, the compounds' structures were refined by assigning atomic types, adding a formal positive charge on the basic groups with the DiscoveryStudio and cleaned-up with a Dreeding-like force field. After that, the Mercury module of the CCDC-suite was used to generate 200 conformers for each compound which were used as the input of a ligand overlay-based pharmacophore modeling run with the Hermes module of the same suite. The obtained overlays were screened on the base of their internal energy and statistical relevance. The most promising pharmacophore model was then visualized both as a 'vector and dot' and a surface-field representation. The experiments conducted for the validation of our *in silico* pharmacophore model were run following the same workflow.

Acknowledgements

This work was supported by Ministero dell'Istruzione, dell'Università e della Ricerca [PRIN 2015.4JRJPP_004] and University of Milan "Piano sostegno alla Ricerca, Linea 2 2018". We also thank the Immunohaematology and Transfusion Medicine Service, Department of Laboratory Medicine, ASST Grande Ospedale Metropolitano Niguarda (Milano) for providing erythrocytes for parasite cultures.

Conflict of interest

The authors declare no conflict of interest.

Keywords: *Plasmodium falciparum* • Resistant strains of *P. falciparum* • Antimalarials • Nanomolar *in vitro* inhibition • *In silico* pharmacophore mapping

References:

[1] R. T. Gazzinelli, P. Kalantari, K. A. Fitzgerald, D. T. Golenbock, *Nat. Rev. Immunol.* **2014**, *14*, 744–757.

[2] World Health Organization, *WORLD MALARIA REPORT 2018*, **n.d.**

[3] O. Miotto, J. Almagro-Garcia, M. Manske, B. MacInnis, S. Campino, K. A. Rockett, C. Amaratunga, P. Lim, S. Suon, S. Sreng, et al., *Nat. Genet.* **2013**, *45*, 648–655.

[4] L. Cui, S. Mharakurwa, D. Ndiaye, P. K. Rathod, P. J. Rosenthal, *Am. J. Trop. Med. Hyg.* **2015**, *93*, 57–68.
[5] S. Romeo, B. M. Dunn, D. Taramelli, E. Bosisio, N. Vaiana, P. Liu, M. Dell'Agli, A. Sparatore, G. Galli, S. Parapini, *J. Med. Chem.* **2006**, *49*, 7440–7449.
[6] S. Romeo, S. Parapini, M. Dell'Agli, N. Vaiana, P. Magrone, G. Galli, A. Sparatore, D. Taramelli, E. Bosisio, *ChemMedChem* **2008**, *3*, 418–420.
[7] N. Vaiana, M. Marzahn, S. Parapini, P. Liu, M. Dell'Agli, A. Pancotti, E. Sangiovanni, N. Basilico, E. Bosisio, B. M. Dunn, et al., *Bioorganic Med. Chem. Lett.* **2012**, *22*, 5915–5918.
[8] A. Pancotti, S. Parapini, M. Dell'Agli, L. Gambini, C. Galli, E. Sangiovanni, N. Basilico, E. Bosisio, D. Taramelli, S. Romeo, *Medchemcomm* **2015**, *6*, 1173–1177.
[9] I. D. K. Untz, K. C. Hen, K. A. S. Harp, P. A. K. Ollman, *Proc. Natl. Acad. Sci. U. S. A.* **1999**, *96*, 9997–10002.
[10] A. L. Hopkins, C. R. Groom, A. Alex, *Drug Discov. Today* **2004**, *9*, 430–431.
[11] A. L. Hopkins, G. M. Keserü, P. D. Leeson, D. C. Rees, C. H. Reynolds, *Nat. Rev. Drug Discov.* **2014**, *13*, 105–121.
[12] D. W. Boykin, A. Kumar, G. Xiao, W. D. Wilson, B. C. Bender, D. R. McCurdy, J. E. Hall, R. R. Tidwell, *J. Med. Chem.* **1998**, *41*, 124–129.
[13] M. T. Makler, J. M. Ries, J. A. Williams, J. E. Bancroft, R. C. Piper, B. L. Gibbins, D. J. Hinrichs, *Am. J. Trop. Med. Hyg.* **1993**, *48*, 739–741.
[14] T. J. Cheeseright, M. D. Mackey, J. L. Melville, J. G. Vinter, *J. Chem. Inf. Model.* **2008**, *48*, 2108–2117.
[15] A. Jahn, G. Hinselmann, N. Fechner, A. Zell, *J. Cheminform.* **2009**, *1*, 1–23.
[16] C. Ghiron, S. N. Haydar, S. Aschmies, H. Bothmann, C. Castaldo, G. Cocconcelli, T. A. Comery, L. Di, J. Dunlop, T. Lock, et al., *J. Med. Chem.* **2010**, *53*, 4379–4389.
[17] A. Nencini, C. Castaldo, T. A. Comery, J. Dunlop, E. Genesio, C. Ghiron, S. Haydar, L. Maccari, I. Micco, E. Turlizzi, et al., *Eur. J. Med. Chem.* **2014**, *78*, 401–418.
[18] M. Sinha, V. R. Dola, P. Agarwal, K. Srivastava, W. Haq, S. K. Puri, S. B. Katti, *Bioorganic Med. Chem.* **2014**, *22*, 3573–3586.
[19] F. K. Brown, P. J. Brown, D. Mark Bickett, C. L. Chambers, H. G. Davies, D. N. Deaton, D. Drewry, M. Foley, A. B. McElroy, M. Gregson, et al., *J. Med. Chem.* **1994**, *37*, 674–688.
[20] W. Trager, J. Jensen, *Science* **1976**, *193*, 673–675.

Discovery and pharmacophore mapping of a new low nanomolar inhibitor of *P. falciparum* growth – TABLE OF CONTENTS

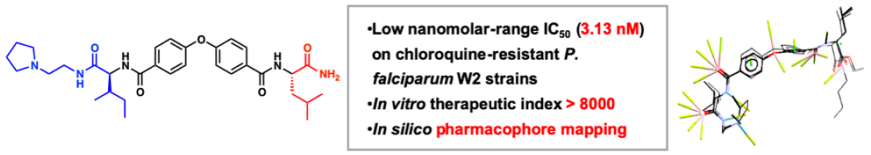

Via an extensive SAR campaign, a new low-nanomolar inhibitor of *P. falciparum* growth was discovered. Its *in vitro* therapeutic index was calculated against healthy human cell lines (HMEC-1) while its metabolic stability was preliminary investigated and assessed as *in vitro* microsomial intrinsic clearance in a murine model. Finally, the peculiar structural features of its novel pharmacophore were deeply investigated by *in silico* studies.